Multi-level analysis of low-cost Z-pinned composite joints: Part 2: Joint Behavior

Javier Toral-Vasquez, Bruno Castanié, Jean-Jacques Barrau, Nicolas Swiergiel

MULTI-LEVEL ANALYSIS OF LOW-COST Z-PINNED COMPOSITE JUNCTIONS.

PART 2 : JOINTS BEHAVIOR

Corresponding author : **Bruno Castanié**

INSA, Département de génie mécanique,135 Avenue de Rangueil,

31077 Toulouse, France.

bruno.castanie@insa-toulouse.fr

Tèl : 33 (0) 5.61.33.81.16

Fax :

MULTI-LEVEL ANALYSIS OF LOW-COST Z-PINNED COMPOSITE JUNCTIONS.

PART 2: JOINTS BEHAVIOR

Javier Toral Vasquez [1], Bruno Castanié[1,2], Jean Jacques Barrau[1], Nicolas Swiergiel[3]

[1] Université de Toulouse, INSA,UPS, Mines d'Albi, ISAE; ICA (Institut Clément Ader),

[2] INSA, 135 Avenue de Rangueil, 31077 Toulouse, France.

[3] EADS IW, 12, Rue Pasteur, 92152 Suresnes

ABSTRACT.

In the framework of ALCAS (Advanced Low-Cost Aircraft Structure) E-U program, a new Z-Pinning technique was developed by EADS Innovation Works. This technology was used to manufacture low-cost Z-pinned junction demonstrators (L and T shaped specimens) typical of aeronautical structures. In order to understand load transfer mechanisms in this kind of assembly, a multi-level analysis was performed. Firstly, tension and shear pin behaviour was investigated as well as pin pull-out from neat resin. It has been demonstrated that the mechanical transfer mode is mainly by bonding even if the pins are twisted. Secondly, an analytical model was proposed which enables to predict the maximum load capability of a single pin. Then, in the second part of this publication, it will be demonstrated that the behaviour of the junction under pull-out, shear and unfolding is globally homothetic to the mechanical behaviour of a pin. Finally this study provides the basis for a design methodology for Z-pinned junctions under complex loading.

KEYWORDS.

A. 3-Dimensional reinforcement, B. Stress Transfer, E. Joints/joining

1-Introduction.

As reported by Mouritz [1], the z-pinning is one of the most promising reinforcement technique for classical laminates. Logically, most of the investigations carried out on z-pinned laminates have focused their attention on the in plane mechanical properties, their delamination behaviour and the impact or post-impact response. However, a little number of authors has investigated the use of the Z-Fiber technology in joints. Lap-joint specimens reinforced by Z-pinning were tested [2] illustrating the behavior of the reinforced joint mainly under shear. It was shown that the static and the fatigue strength were both increased by 40 %. However, this result depends on the density of pinning, in this case 2%. Delamination appears for lower densities and higher densities where a static failure occurs at the border of the pinned zone. The same order of magnitude in the strength increase was obtained by Grassi et al [3] for joints in pipes. In order to increase the shear strength of such a joint, the idea of using inclined pins were analysed by Rugg et al [4]. For +/- 45° angle and the configuration studied, the static strength were increased by 100%. Nevertheless, the crack initiation at the interface is only slighty influenced by the pins. One interesting point is the fact that the mechanical behavior of the pins is very different where pushed or pulled depending on their relative orientation to the applied load: pins been pulled disbond easily while pins been pushed support high shear load level before failure. However, no influence of pins inclination have been observed by Chang et al [5] for lower inclination angles between 13º and 23º and for temperatures bellow 150ºC.

Z-fiber technology has also been considered for increasing joint behaviour of aeronautic joints. Nevertheless, the only known application is the reinforcement of skin to stiffener joints of F/A-18 E/F "Super Hornet" [6]. This kind of reinforcement on co-cured stiffener feet has been investigated by analogy through DCB tests by Byrd and

Birman [7-8]. T-joint pull-out tests have also been performed by Rugg et al [9]. Depending on the web to support distance, delamination starts at the web root or at the flange end what can be justified by energy balance analysis. Cartié et al [10] have compared experimentally T-joints tufted and pinned and also proposed a model based in fracture mechanics. By knowing the cracks propagation paths and using a linear mixed mode criterion, the authors were able to correlate experimental load/displacement curves. Greenhald et al [11] have investigated pinned T-joints behaviour under pull-out showing a load carrying capacity 229% higher than the baseline. However, delamination initiation load level is only slightly affected. In summary, unlike stitched joints ([12]-[15]), few studies have focussed their attention on composite structures joint by pinning. It is true that Z-Fiber ® is constraint to be applied principally to stiffeners foot to skin joints, EADS IW technology [16] allows deeper pin insertion and thus new junctions' designs can be investigated. In this part of multi-level analysis, representative specimens of typical aeronautics joints have been used to evaluate pin contribution to static behaviour and to propose a modelling methodology.

2- Experimental analysis.

2.1 Specimen and test description.

L and T shaped specimens, most typical for aeronautical joint were chosen for this study. The specimens were manufactured following the description made in the first part of this article and in [16]. L-joints geometry is presented in Figure 2. The skin is manufactured from UD Uniwave PRIFORM IMS 200 plies with the following stacking sequence: $[90/45/0_2/45/90/-45/0_2/45/0/-45/0/45]_s$ for a total thickness of 7 mm and where 0º plies are parallel to specimen length (see figure 2). The vertical part attached to the skin corresponds to a rib foot. It is manufactured from NCF PRIFORM HTS 450

with a theoretical thickness of 3.8 mm. The skin to rib-foot interfaces is 0º/0º. Two pin lengths are investigated: 15 and 40 mm. Pinning pattern is presented in Figure 3 with 3 staggered rows clearly appreciated over the lower skin surface. It must be pointed-out that pin insertion produces a wavy effect in the highest plies of the skin over the joining line (figure nº 4). For L-joints, outer radius of the rib-foot is filled with a UD fillet along the width of the specimen (see Figure nº 4). Five joint configurations have been investigated:

- Non pinned L-joints: type A
- 15 mm pinned L-joint: type B.
- 40 mm pinned L-joint: type C.
- 15 mm pinned T-joint: type D.
- 40 mm pinned T-joint: type E.

Specimens are tested under pull-out, shear and bending. Three specimens are tested for each loading so 45 tests are performed in total. Boundary conditions for all the loadings and all configurations (except type B, D and E under tension) consist in clamping the skin 5 mm away from the web and the foot end. The load is applied over the web: tension and bending (Figure nº 6) and shear (figure nº 7). Shear test has been conceived to apply the load at the skin-to-web interface.

Tension and bending tests are instrumented with cameras over both sides of the specimen so crack initiation can be detected using plane image correlation technique through Correli® software [18]. Load application point displacements are measured by two LVDT sensors. Applied load have been measured through 100 kN load cell and displacement ratio is fixed to 0.2 mm/min.

Within this paper, the authors have focused on maximum applied load results and behaviour as they are more impacted by pins presence. However, extra analyses are per-

formed to investigate cracks initiation [17]. The results from this analysis are in line with previous studies where crack initiation is found to be only slightly influenced by pinning [11]. This is also the conclusion of stitched T-joints studies [13]. In addition, for the presented technology, some specimens present cracks at the interface before loading so no conclusion can be extracted. It has been demonstrated by using thermal FEM analysis that cracks appear due to thermal loading over a resin rich area [17].

2.2 Pull-out tests results and analysis.

Load/displacement curves for non pinned L-joints are shown Figure Nº 8. A first irregular response appears up to 500N corresponding to the specimen positioning stage followed by a regular applied load increase until the final sudden failure. Failure load level is highly dependent on the presence of cracks in the specimen before testing. Indeed, correlation image analysis has shown that specimen 1 presented a crack along the whole width of the skin/rib-foot interface at 200 N [17]. This crack grows and reaches 7 mm long when applied load reaches its maximum level. It is highly likely that crack appeared during manufacturing process. On the other hand, for specimen 3, no crack has been detected before failure and thus, load increase appears to be very regular and failure occurs without previous signs. Specimen 2 behaviour is between specimen 1 and 3 as no crack has been detected before failure but final delamination occurs through different plies interfaces what may indicate that crack was non visible. To sum up, tension failure load is 2806 N +/- 789.

Figure 9 shows typical load/displacement response of configuration C (pinned L-joint, pins 40 mm long). In this case, scatter is lower than non-pinned configuration with a maximum applied load of 5598 +/- 463 N, which represents a 100% increase. Pinned L-joints show cracks appearing on the skin/rib-foot interface at the same load order of

magnitude than non-pinned joints (point I). Then, crack propagates along the interface while load goes on increasing (point II). It can be concluded that, during this stage, tension load is mainly carried by pins. Finally, after a first load drop, load decrease slowly while pins slip from skin until total pin pull-out (III). Same behaviour has been observed for configuration B which maximum applied load is 4955 +/- 355 N.

Pinned T-joint behaviour is similar to pinned L-joints. Due to low interface surface between skin and web, premature cracks are present so only pins carry the tension load. The results of pull-out test are summarized in Figure nº 10. Globally, it can be observed that for both pinned L and T-joints and for the two insertion depths investigated, the results are equivalent within a +/- 10% range. The differences are due to different boundary conditions for configuration C [17], and to the fact that, for configuration B, 15 mm pins are inserted in a resin-rich region of the interface leading to a less effective load transfer capability. For all configurations, it has been observed that pins are not exactly perpendicular to the skin what could generate extra scatter. From all test performed, the mean maximum carried load by one pin is equal to 300N. This value is perfectly consistent with results from analytical model presented in the first part of this study that gives 336 N for a 7 mm pin insertion depth. What's more, pin mean load scatter is lower than scatter from single pin tests probably due to the RTM process producing more homogenous joints. This last remark validates the initial assumption of the homothetical response of pinned joints compare to a single pin.

2.3 Bending tests results and analysis.

Load/displacement curves for non pinned L-joints are given in Figure Nº 11. Failure appears suddenly without any appreciable previous crack propagation. Specimen post-mortem appearance is given also in Figure 11. Failure occurs when a crack appears

at the outer radius over the UD fillet and propagates through the foot to skin interface. Maximum applied load reaches 728+/-48 N.

Load/displacement curves for pinned L-joints with 40 mm pins are shown Figure 12 and the related behaviour is described hereafter:

1.Non linear web deflexion until reaching 1848 N of mean applied load (before first load drop in I). A crack appears and propagates over 8mm through the plait and the foot to skin interface (see Figure 12). During this stage, pins debond slightly from the skin. The combination of these two phenomena explains the non linear response

2.Load drop at point I (Figure 12) correspond to the delamination in the radius of the rib-foot. In this area, peeling and interlaminar shear stresses are high and, in addition to this, plies geometry is disturbed by pins insertion.

3.Second load drop is due to the failure of plies in the inner area of the radius under compression loads. Compression failure is a consequence of delamination described in 2 as it leads to a local bending stiffness decrease and so, a redistribution of tension and compression stress. Post-mortem section shows this failure (Figure 13) and also pins debonded from skin under bending.

Bending strength is 1842+/-58N which represents an increase of +153% compared to no-pinned L-joints. L-joints reinforced with 15mm long pins show a very different behaviour as given in Figure 14. Crack appears far over the fillet and propagates from there through the web/fillet interface until reaching the skin/foot interface. In this case, pins are not long enough to be correctly inserted in the web and carry bending loads. Thus, failure load decrease to 801+/-76N, representing 10% increase from no-pinned L-joints.

Bending Load/displacement curves for T-joints pinned with 40 mm long pins are shown in Figure 15. A first linear load increase is observed until 165 N where a plateau

appears. Visual analyses show that this happens when outer pins star disbonding from the skin and continue slipping from it. The load plateau extends until the displacement reaches 17 mm. At that moment, rotation angle at the web base is too high and pins fail by bending making load to drop-off.

Bending failure load for each configuration is shown Figure Nº 16. Under bending load, pins length is an important parameter as only joints reinforced with 40 mm pins have shown a significant improvement. In that case, due to their insertion depth into the web, pins increase stiffness and also the strength. Pinned T-joints are not effective under bending due to their natural low mechanical strength. T-joints reinforced with 15 mm pins are slightly more resistant than the ones reinforced with 40 mm pins. However, the difference is thought to be due to the fact that T-joints with 15 mm pins have their three rows more widely spaced that 40mm pins T-joints, which increase bending stiffness and strength.

2.4 Shear tests results and analysis.

Figure 17 shows load/displacement curves from L-joints shear tests. Globally, pinned and no-pinned L-joints present the same failure scenario described hereafter: firstly a delamination (point A) appears over the opposite side of the applied load. Indeed, a parasite bending moment is produced as the application load direction may not be perfectly aligned with the specimen interface (figure Nº 18). However, delamination starting point could be different depending on configuration and initial specimen defects. It can appear inside the fillet or at the end of the stiffener foot [17]. After first delamination, a stiffness decrease can be observed as the cracks grow at the interface (point A to B, Figure N°17). Crack path is complex and it can go through a pair of plies interface to the higher or lower one [17]. Finally, specimen fails suddenly because of a fast delamina-

tion propagation in case of unpinned L-joints, or because of pin shear failure in case of pinned joints. Post-mortem analysis of pinned joints over a section of pin rows shows that most of pins have debonded before shear failure except for the ones under compression load generated by the parasite bending moment (Figure 18). Besides, no influence of pin length has been observed over failure mode or load/displacement curves [17]. This observation has been confirmed in terms of maximum applied load as they are exactly the same for both L-joints with 15 and 40 mm pins (Figure Nº 20). Figure Nº20 also shows that pin reinforcement increase only 20% mean shear strength.

T-joints failure mode seems to be different: although delamination appears on the web to skin interface, it does not lead to a stiffness decrease. Some stiffness drops-off are observed over the load/displacement curve (Figure 19) but they are linked to the same pin debonding scenario as for L-joints as it has been deduced from specimen post-mortem analyses. T-joints pinned with 15 mm pins show a maximum carried load 15% higher than T-joints reinforced with 40 mm pins. It has also been observed that pins misalignment angle impacts strongly on shear strength. Curves on Figure nº 19 show a higher strength of specimens whose pins are oriented with the direction of the applied load. In that case, pins are mostly loaded on tension (pull-out) what increase joint strength. On the other side, when pins are oriented against the applied load, the shear component is higher and it makes the joint become weaker. On both cases, a higher strength has been observed for T-joints reinforced with 15 mm than 40 mm. The higher web stiffness due to pinning of 40 mm deep could produce additional loads at the interface that penalizes carrying load capability.

When comparing L-joint solution with T-joint configuration, L-joint strength remains far over T-joint's as the interface surface is much higher.

2.4 Conclusions.

Tests performed over T and L-joints with and without pinning reinforcement have made possible to analyze their behaviour under three static loadings: tension (pull-out), shear and bending. The results of this study will allow a future designer of this kind of joints to orientate his choices in terms of configuration. The parameters investigated (T or L shape and pin length) have an impact on joint behaviour but not necessarily under all loadings. For example, pin length has an impact on bending behaviour but modifies only slightly tension and shear response. Generally speaking, for test performed, pinned L-joint configuration shows a better behaviour that T-joint. However, this assertion could not be any more valid for complete stiffened structure where T-joints could be reinforced with inclined pins [19]. Regarding the type of effort on the pins, they are always loaded under tension and they always fail by debonding from the skin: the thinner part where they are inserted. This means that pin debonding load is a good indicator of joint strength and allows comparison. Moreover, experimental mean pin pull-out load values match well with the prediction from the analytical model presented on the first part of this publication. It validates multi-level approach and allows to feed the model proposed in the next paragraph.

3- Computation of the strength of Z-pinned Junction.

3.1 Modelling principles.

The purpose of this section is to present a modelling methodology able to predict pinned joint strength. Experimental analyses have shown, with only one exception, that rib-foot to skin interface is broken on the pinned area before final joint failure. This observation is not verified for pinned L-joints under shear. Indeed, joint failure appears suddenly and it has not been possible to identify latest failure scenario: pins, interface or

a mix. Moreover, in this case, interface surface is large enough to carry a significant part of the load so the real load distribution between pins and interface can not be obtained with a presizing model as presented here. In fact, this problem is similar to the bonded/ bolted joints behaviour for which a significant and specific research work needs still to be done ([20];[22]). For this reason, only T-joints will be modelled under shear as the interface area remains small.

General approach is described on Figure 21: interface is supposed to be broken and thus, web and skin are only joined by pins. Pins are represented by non-linear springs which tension and shear behaviour laws are obtained from elementary test presented in the first part of this publication. Within the next section, this general approach will be applied to the variety of specimens and loadings investigated.

3.2 Tension and bending.

Tension and bending tests over L-joints have been simulated with a 2D model presented in Figure 22. Skin and rib-foot are meshed with quadrangular elements taking into account plies orientation and considering plain strain. Pins have been represented by 1D elements (rods) with an equivalent section corresponding to the pin section per specimen width unity. Pin nodes are coincident with skin and web ones. At the skin to rib-foot interface, pins are modelled according to the principle described in section 3.1. Material properties applied to the different parts of the model are given in table 1. In terms of boundary conditions, the skin is considered clamped 10 mm away from the web or the end of the rib-foot. Loading under tension has been simulated by applying a vertical displacement over the web. For bending, a horizontal displacement has been applied to the web.

Figure 23 shows load/displacement curve obtained by simulation and the one obtained from pinned L-joint tension test. Despite of a higher stiffness for the simulation results, a good agreement has been found between both curves, especially in terms of maximum applied load. The stiffness mismatch could be due to an insufficient clamping action at the skin during the tests. Indeed, while tightening clamping plates over the skin ends, some parasite stress concentration appear on the rib-foot to skin interface due to specimen geometrical defaults. In order to avoid this parasite loading, it has been decided to be used a light clamping load.

Load/displacement curve obtained from FEM shows an irregularity for 4760N. It corresponds to the debonding of the most outer pins row. Thus, from that moment, pins of the first row carry only the load by friction. Thereby, the model allows estimating the load level that produce first debonding of the pins that should correspond to the limit load. In terms of maximum applied load, the model predicts 5343 N, only 5% lower than mean experimental value of 5598 N. The difference is lower than experimental scatter.

Regarding pinned T-joints under tension, the model strength estimation is 5560N, 10% over mean experimental measurement. The difference remains acceptable taking into account the scatter observed in elementary pin pull-out tests. The model predicts a simultaneous disbonding of the three pins rows at the maximum applied load.

Pinned L-joint model under bending (folding) is quasi-identical to the one used for tension (see Figure Nº 22). The only difference comes from the fact that, for bending, the interface is considered to be delaminated only at the pinned area from the web to the beginning of the rib-foot. This delamination length can be justified by analysing bending test results where it has been observed that joint failure occurs when rib-foot brakes before the total delamination of the interface [17].

Figure 24 shows load carried by the three pin rows as a function of the displace-

ment of the load application point. On the same graphic, total joint carried load from tests and from the simulation are also plotted against load application point displacement. A good agreement between test and calculation can be observed even if the model doesn't represent delamination growth. Load carried by the three pins "row 1", "row 2" and "row 3" can be read over the right vertical axis whereas total load values correspond to the left vertical axis. According to the simulation, pins from row 1 (on the left on Figure 22) start disbonding when the applied load reaches 420N. Thus, this load level will correspond to the joint limit load as, for higher loads, pins on row 1 will carry load just by friction. Once the third row debonds at an applied load around 1100N, joint bending stiffness change and its integrity is only assured by the skin to the end of the rib-foot interface. Nevertheless, pins still carry some load by friction. From a sizing point of view, the failure of the joint can be consider occuring at 1100N even if total failure happens for a higher load level.

Regarding T-joint under bending, Figure 25 shows simulation results versus three test measures. Simulation curve matches globally well with experimental results. However, a difference on the slope change can be observed for an applied load of 150N. Indeed, the model shows two slope changes at 115N and 150N corresponding to the first and second pin row debonding. Tests have only shown one slope change for a mean load value slightly higher: 165N. The difference can be explained as the model considers a perfect geometry and identical pin pull-out laws. In reality, pins are not exactly over their theoretical position and small deviations can impact bending strength.

In this way, it has been shown that FE model proposed allows calculating pin joint strength under tension and bending loadings.

3.3 Shear.

T-joint pinned with 40 mm pins over three rows has been simulated with a 3Dmodel shown in Figure 26. Like for pinned L-joint under tension, only pins have been represented by non-linear springs at the web to skin interface. Material properties are the same as in previous models (Table 1). Boundary conditions are also clamping conditions over the skin 10 mm away from the web. Load application test rig has been modelled by rigid elements. Contact at the web to skin interface has been considered in order to avoid web elements to penetrate into the skin on the compression area.

Simulation results are compared to test measures on Figure 27. It must be reminded that pinned T-joints shear behaviour depends on relative pins angle against applied load. Thus, on the same graphic, the shear responses of specimens with 40 mm pins oriented "against" and "towards" de load are plotted. The model response shows stiffness slightly lower than the test measures. The difference could be due to the fact that the model does not represent the resin layer between web and skin. This layer could stiffen the specimen even if it delaminates during the test. The simulation stops suddenly when shear load on the most loaded pin reaches the pin shear strength. Model maximum applied load is coherent with test results.

Figure 28 shows axial and shear load carried by three pins as a function of the load application point displacement. "Pin 1" corresponds to a pin on the lowest side of the interface (lowest Z coordinate value) where tension load over the pins are higher due to the bending parasite moment. On the other side, "pin 6" is placed on the highest side of the interface, closer to the ball-joint used to introduce de load. On the graphic, the total applied load is also plotted in order to better understand the response of each pin compared to the global joint response. Load on pins can be read on the left vertical axis and joint global applied load over the right one. According to the simulation, the first pin to

debond is "pin 1" over the lower part of the specimen for an applied load level of 2000N, a low value compared with joint shear strength. "Pin 6" is firstly loaded under compression but axial load changes it sign to tension load when the joint applied load reaches 2500N. Pin 6 debonds when applied load is 4000N. From that moment, pins carry tension load only by friction. At the same time, pins are also loaded under shear by forces increasing gradually with shear total applied load. Joint failure occurs when shear load over pins 6 and 3 reaches the shear strength (298 N). It can be observed that maximum shear pin load is reached almost at the same time over all the pins what explains the sudden specimen failure.

The simulation shows pins to be loaded mostly under tension. It could explain why the maximum applied load obtained from the model is in line with shear strength of specimens with pins oriented "towards" the load. Indeed, experimentally, as pins are inclined towards the applied load, they are more loaded in tension and it will produce a higher joint strength.

The proposed model allows representing only one of the configurations tested due to the particular behaviour of pinned joints under shear when pins are not perpendicular. Numerical studies have allowed to represent T-joints pinned with pins oriented "against the load" by leading to a lower shear strength. However, these results have been obtained by modifying original single pin behaviour laws obtained in the first part of this paper. In particular, single pin response under combined loading (shear/tension, shear/compression) should be investigated in detail in order to feed a more capable finite elements model.

4- Conclusions.

For this study, pinned joints behaviour manufactured with EADS Innovation Works has been investigated. This technology allows manufacturing composite sub-assembly including skin/stiffener joints with a high integration level.

In this paper, experimental behaviour of pinned and non-pinned joints under static tension, shear and bending loading has been analysed. Two main joint families has been tested: L-joint (classical design) and T-joints (lower manufacturing cost consuming)

Globally, for all the configurations, pins increase joint strength strongly (more than 200% for L-joints under tension and bending). The benefit is lower under shear. The comparison between classical non pinned L-joint and pinned T-joint have shown that pinned pull-out and shear T-joint capabilities can be as good as non pinned L-joints but with a lower associated manufacturing cost. This is not the case for bending where T-joint strength is low. Joint behaviour under shear is highly dependent on pins misalignment produced during the manufacturing process. This phenomenon could be avoided by using a pin pattern with alternative inclinations as proposed in [19].

Pinned joint mechanical behaviour simulation has shown the validity of multi-level approach. A good agreement between test results and model prediction has been found in terms of tension and bending strength. Joints behaviour under shear is globally well captured by the model in case of pins oriented "towards the load". In order to obtain a more universal model, investigations on pins behaviour characterisation under combined loading should be done. From a numerical point of view, it could be interesting to switch from a model based on spring elements to a model using specific cohesive elements still to be developed. Indeed, cohesive elements allow an easier application on the simulation of big structures where spring-base models can be very hard to implement.

From a general point of view, this study represents the first stage on the under-

standing of the mechanical behaviour of this new technology. Although first characterisations have been done here and even a model has been proposed, a significant work must be done still before the technology is mature enough to be used in an industrial project.

5-Acknowledgement.

Authors would like to thanks Thierry Vilain (Dassault Aviation and ALCAS WP3 leader) and Patrice Lefebure (EADS IW) for their support.

6-References.

[1] Mouritz A.P.: Review of z-pinned composie laminates. Composites Part A 2007; 38(12): 2383-2397.

[2] Chang P, Mouritz AP, Cox BN, Properties and failure mechanisms of pinned composites lap joints in monotonic and cyclic tension. Composites Part A ,2006.

[3] Grassi M, Cox B, Zhang X, Simulation of pin-reinforced single-lap composite joints. Composites Science and Technology. 2006.

[4] Rugg KL, Cox BN, Ward KE, Sherrick GO, Damage mechanism for angled through thickness rod reinforcement in carbon-epoxy laminates. Composites Part A 1998; 29(?) :1603- 13.

[5] Chang P., Mouritz A.P., Cox B.N., Elevated Temperature Properties of Pinned Composite Lap Joints. Journal of Composite Materials, Vol. 42, 2008.

[6] Exline G. Z-Pins strengthen Super Hornet structures, save weight and cost. The integrator 2001; 3: 1,3.

[7] Byrd L.W., Birman V. Effect of temperature on stresses and delamination failure of z-pinned joints. *International Journal of Mechanical Sciences 48 (2006) 938–949*

[8] Byrd L.W., Birman V. Effectiveness of z-pins in preventing delamination of co-cured composite joints on the example of a double cantilever test. *Composites Part B: Engineering, Volume 37, Issues 4-5, June-July 2006, Pages 365-378*

[9] Rugg K.L., Cox B.N., Massabo R., Mixed mode delamination of polymer composite laminates reinforced through the thickness by z-fibers. Composites Part A 33 (2002) 177-190.

[10] Cartié D.D.R., Dell'Anno G., Poulin E.,, Partridge I.K., 3D reinforcement of stiffener-to-skin T-joints by Z-pinning and tufting, Engineering Fracture Mechanics 73, pp 2532-2540, 2006

[11] Greenhalgh E., Lewis A., Bowen R., Grassi M. Evaluation of toughening concepts at structural features in CFRP – Part I: Stiffener pull-off. Composites Part A 2006; 37(10): 1521-32.

[12] Reeder JR, Glaessgen EH, Debonding of Stitched Composite Joints Under Static and Fatigue Loading, Journal of Reinforced Plastic and Composites, Vol. 23, No 3. 2004.

[13] Stickler PB, Rumalu M, PS Johnson, Experimental and numerical analysis of transverse stitched T-joints in bending. Composite Structures 50, pp 17-27, 2000.

[14] Stickler PB, Rumalu M, Investigation of mechanical behavior of transverse stitched T-joints with PR520 resin in flexure an tension. Composite Structures 52, pp 307-314, 2001.

[15] Stickler PB, Rumalu M, Parametric analysis of stitched composite T-joints by the finite element method. Materials and Design 23 pp 751-758, 2002.

[16] Lefèbure P., "Assembly of dry Carbon Preforms by a Z-pinning technology", SAMPE Europe Technical Conference, SETEC January 2006.

[17] Javier Toral Vasquez. Identification et modelisation du comportement des structures composites assemblees par cloutage. Thèse Université de Toulouse. http://the-

ses.supaero.fr/001428.pdf (in french).

[18] F. Hild, J.N. Périé, M. Coret, Mesure de champs de déplacements 2d par corrélation d'images numériques : correli^{2D}, rapport interne LMT Cachan, 230, 1999.

[19] C. Petiot. New challenges in structural design and analysis of composite structures. CEAS European Air & Space Conference, 2007. Berlin, Germany, 10-13 September 2007.

[20] Fu M., Mallick P.K. Fatigue of hybrid (adhesive/bolted) joints in SRIM composites, International Journal of Adhesion and Adhesives. 21, pp. 145-159, 2001.

[21] Kelly G. Load transfer in hybrid (bonded/bolted) composite single-lap joints. Composite Structures 69 (2005) 35–43.

[22] Paroissien, E., Sartor, M., Huet, J., & Lachaud, F., Analytical two-dimensional model of a hybrid (bolted/bonded) single-lap joint, Journal of Aircraft, AIAA, Vol. 44, No. 2, p. 573-582, March-April 2007.-

FIGURES

Figure N°1: EADS IW pinning structure of T and L joi nts.

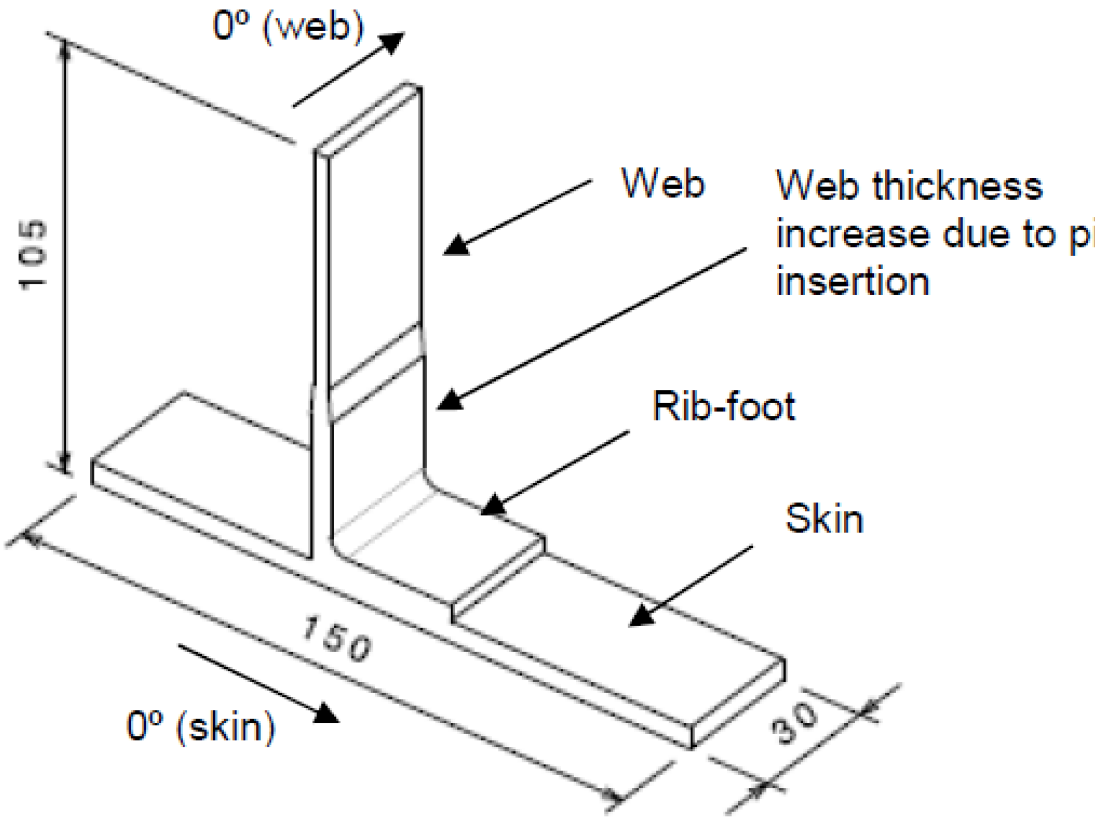

Figure N°2: L-joints geometry.

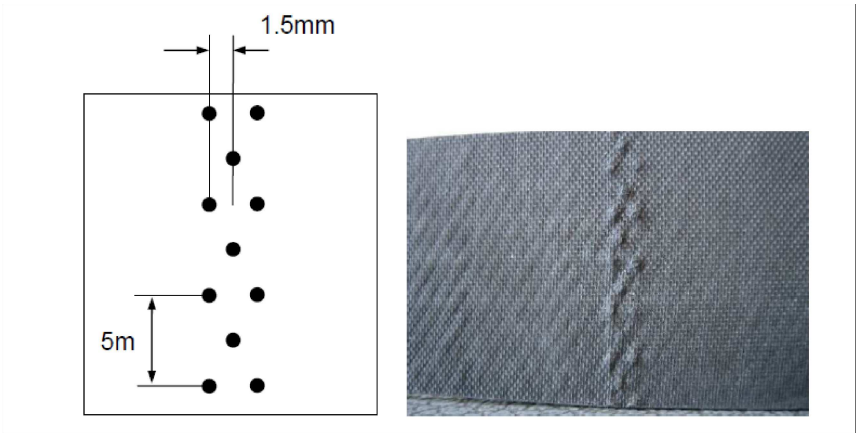

Figure N°3: Pin pattern diagram (left) and on speci men lower skin surface (right).

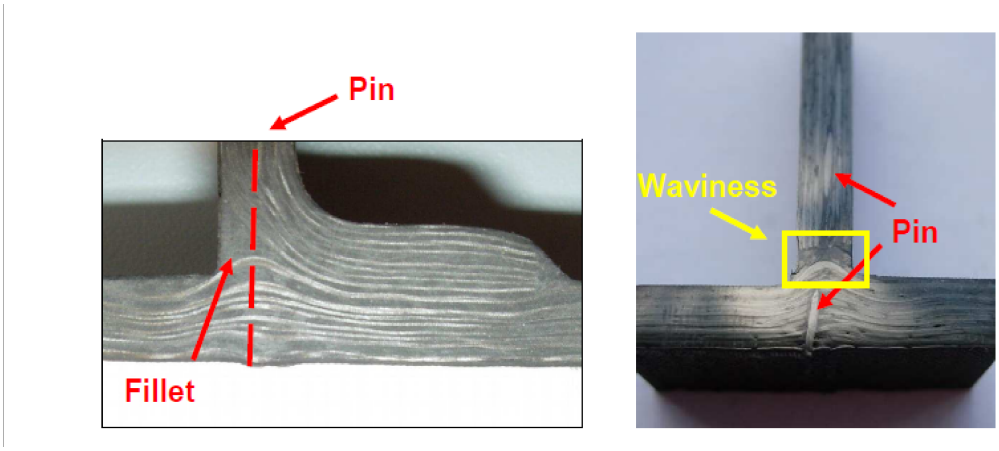

Figure N°4: Waviness created by the pin insertion.

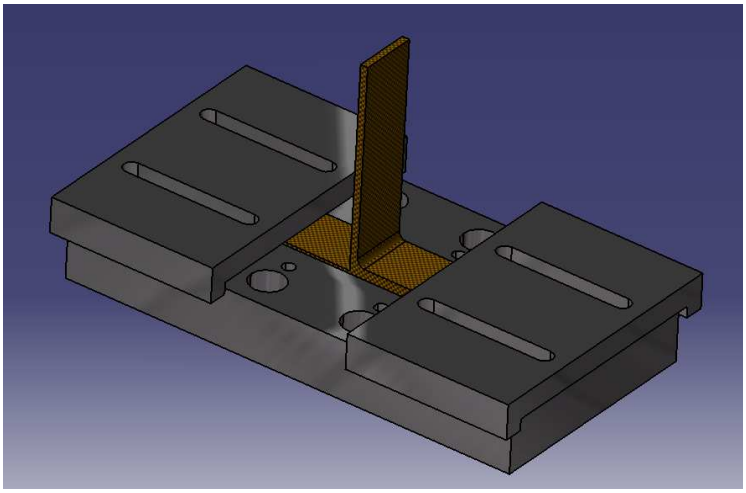

Figure N°5: Universal test rig.

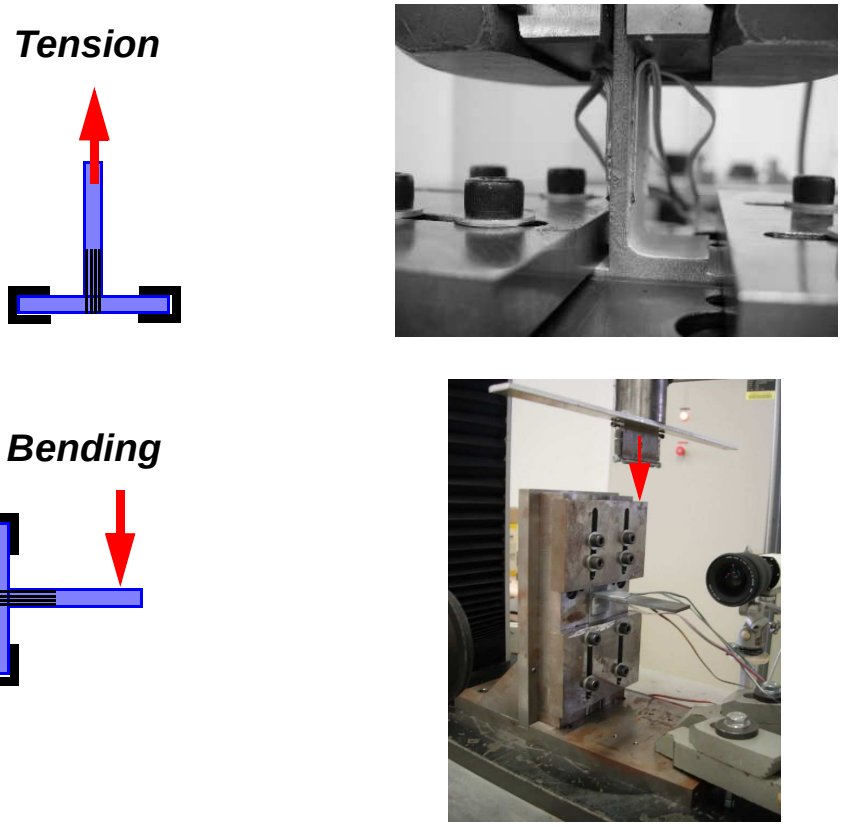

Figure N°6: Traction and bending test description.

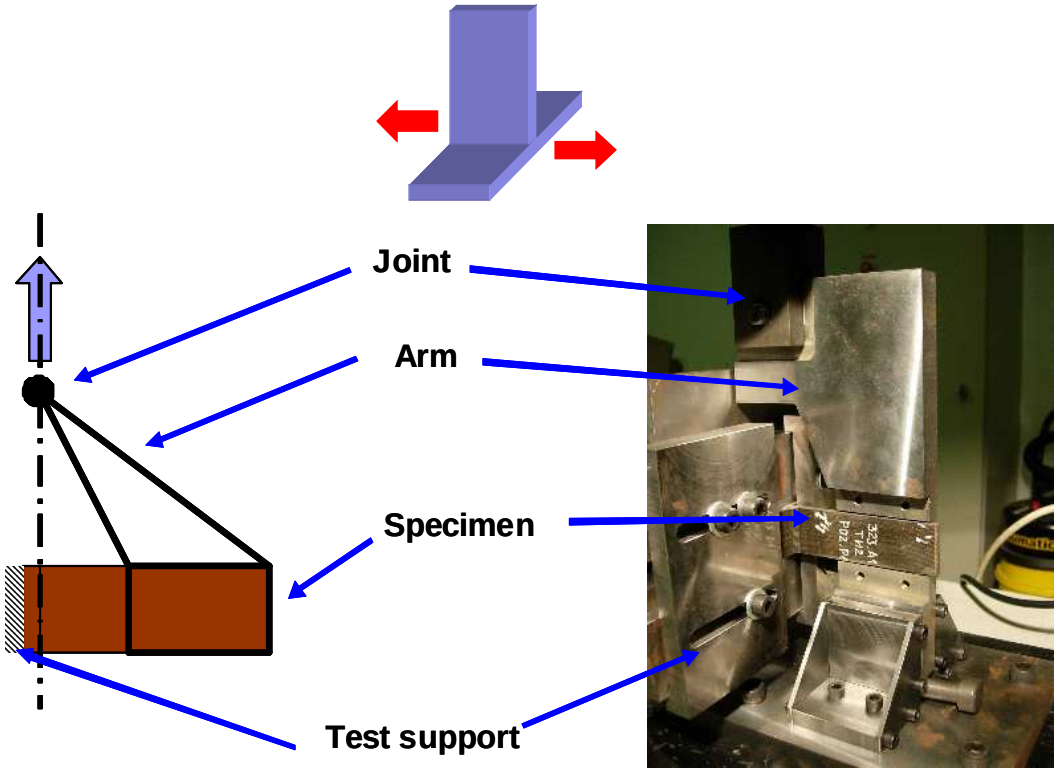

Figure N°7: Shear test description.

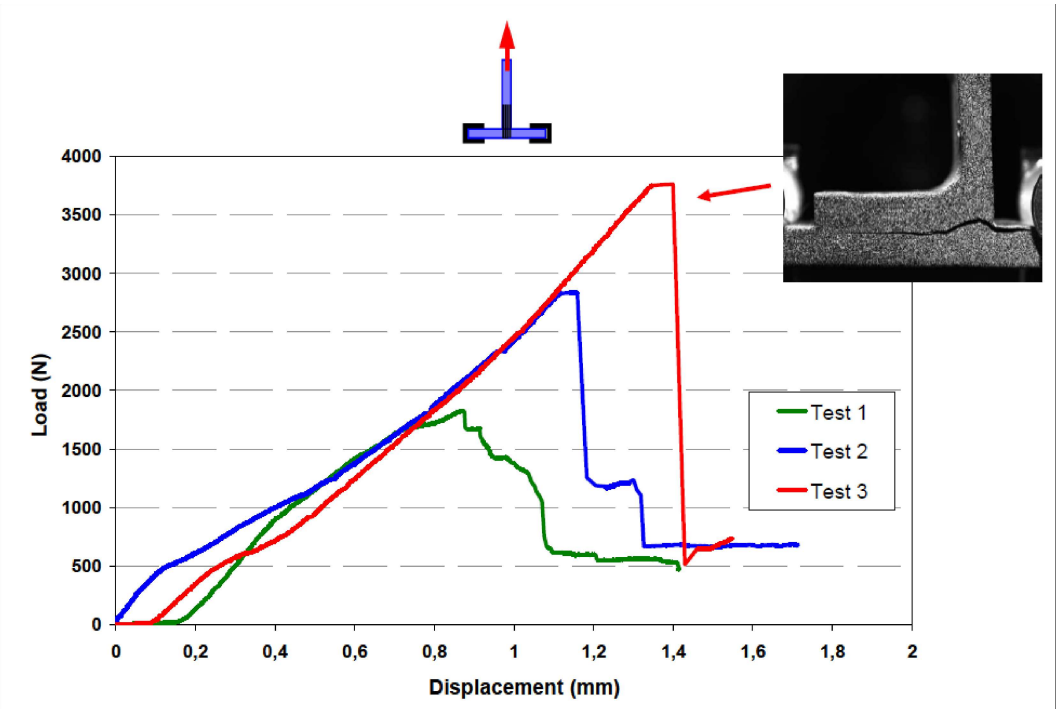

Figure N°8: Non-pinned L-joints tension tests load/d isplacement curves.

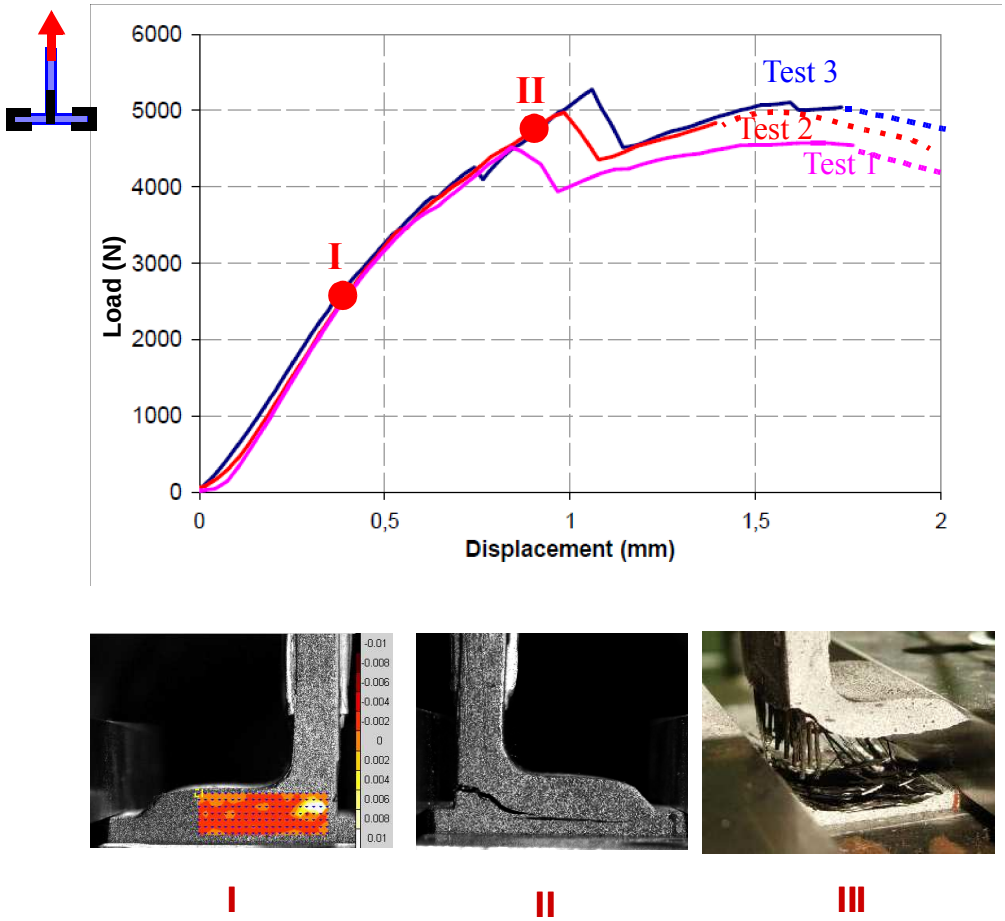

Figure N°9: Pinned L-joints (40 mm pins) under tens ion): load/displacement curves and failure scenario.

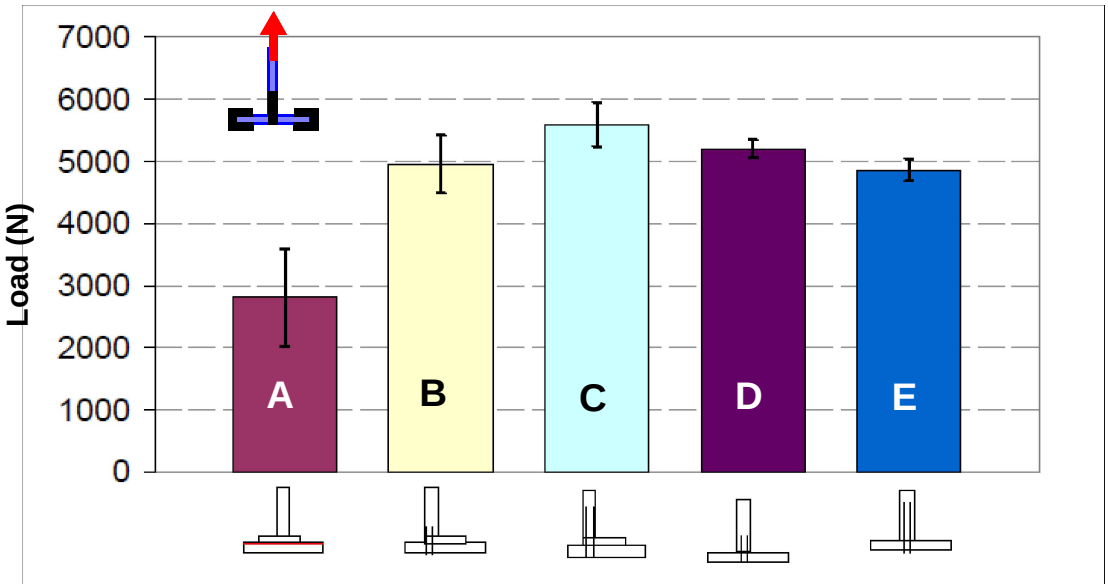

Figure N°10: Maximum load for tension test on L and T-joints.

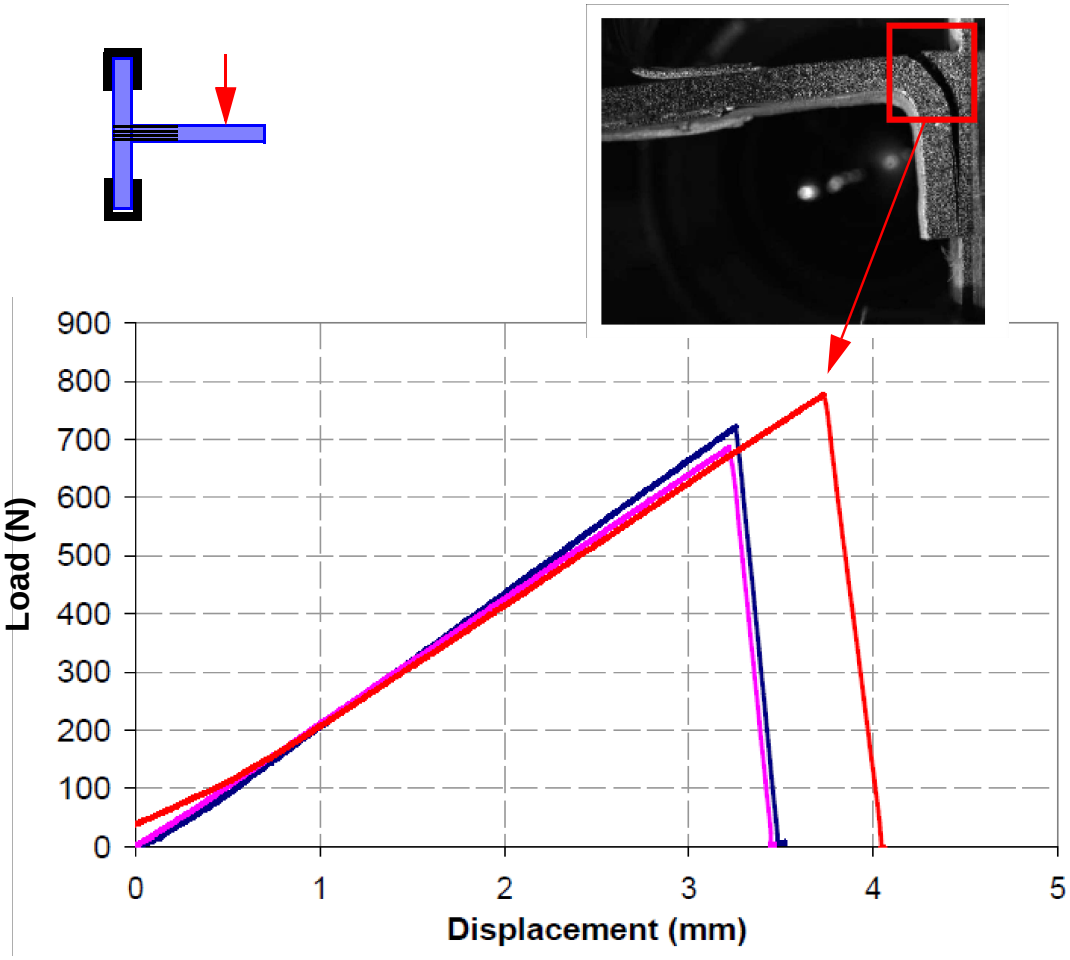

Figure N°11: Load/displacement curves for bending o n non-pinned L-Joints.

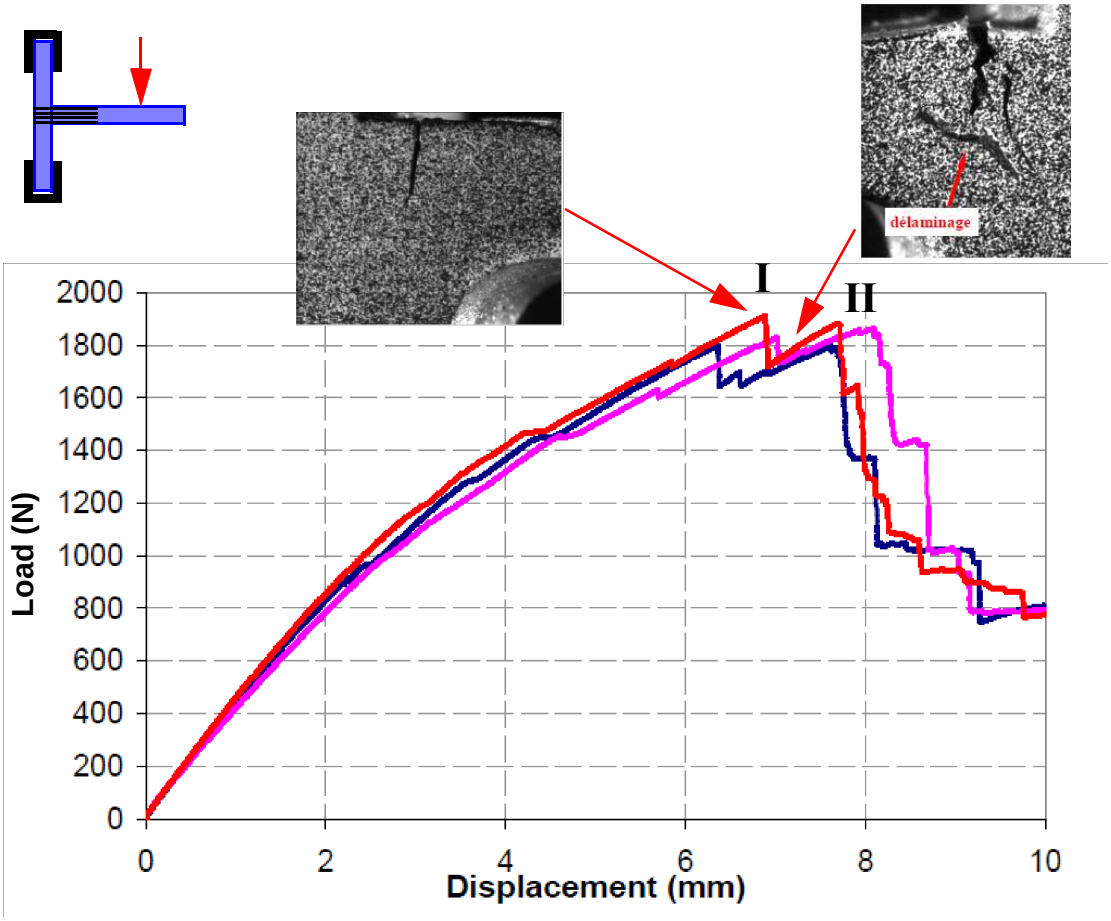

Figure N°12: Load/displacement curves and failure s cenario for bending of L-joints pinned with 40 mm pins.

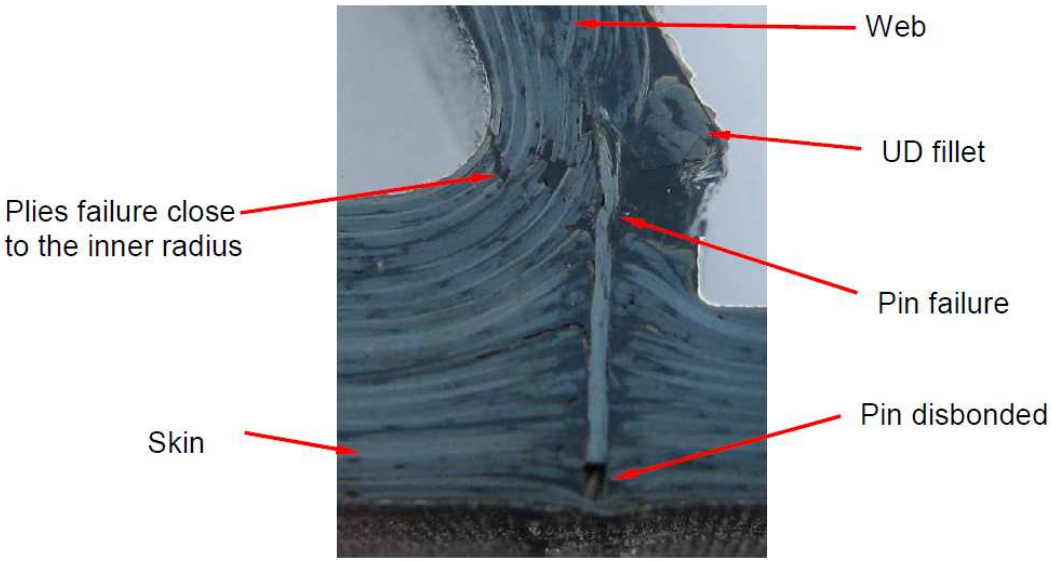

Figure N°13: Post-mortem specimen lay-out of 40 mm pinned L-joint under bending.

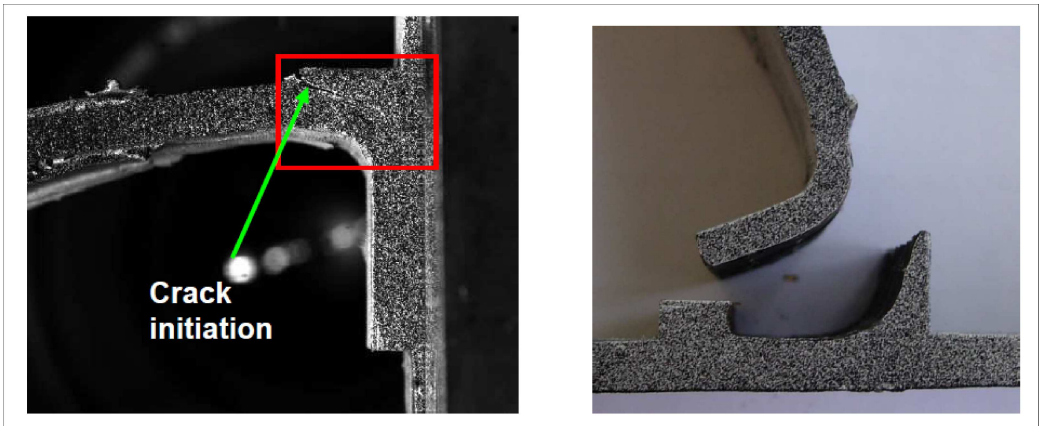

Figure N°14: Failure initiation and final failure p attern for 15 mm pinned L-joint under bending.

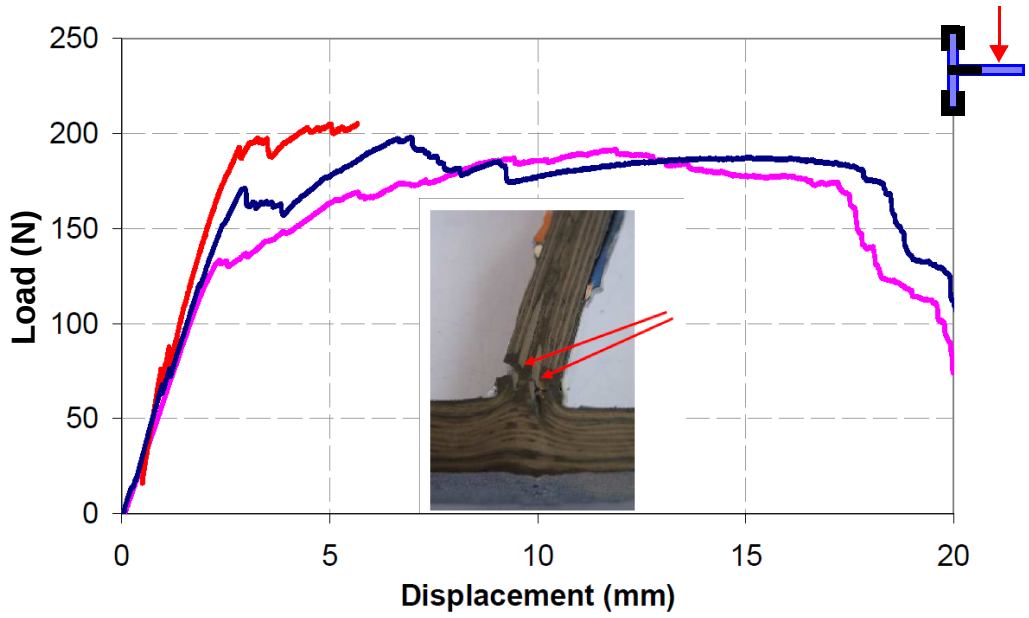

Figure N°15: Load Displacement curves and failure sc enario of 40 mm pinned T-joints under bending

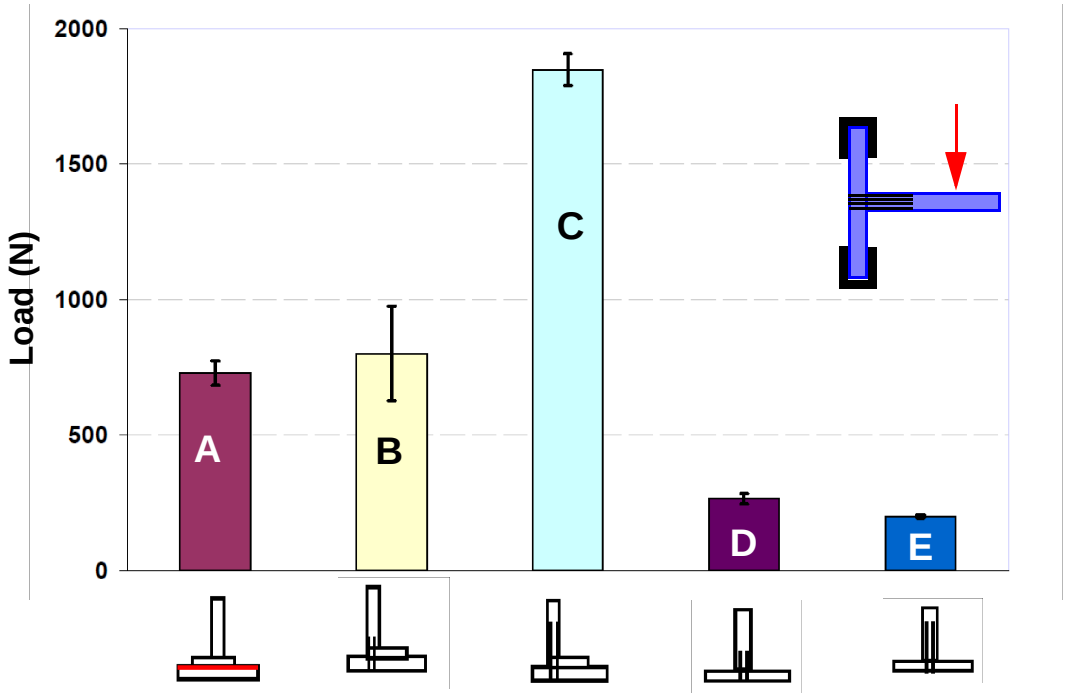

Figure N°16: Bending tests maximum applied load for L and T-joints.

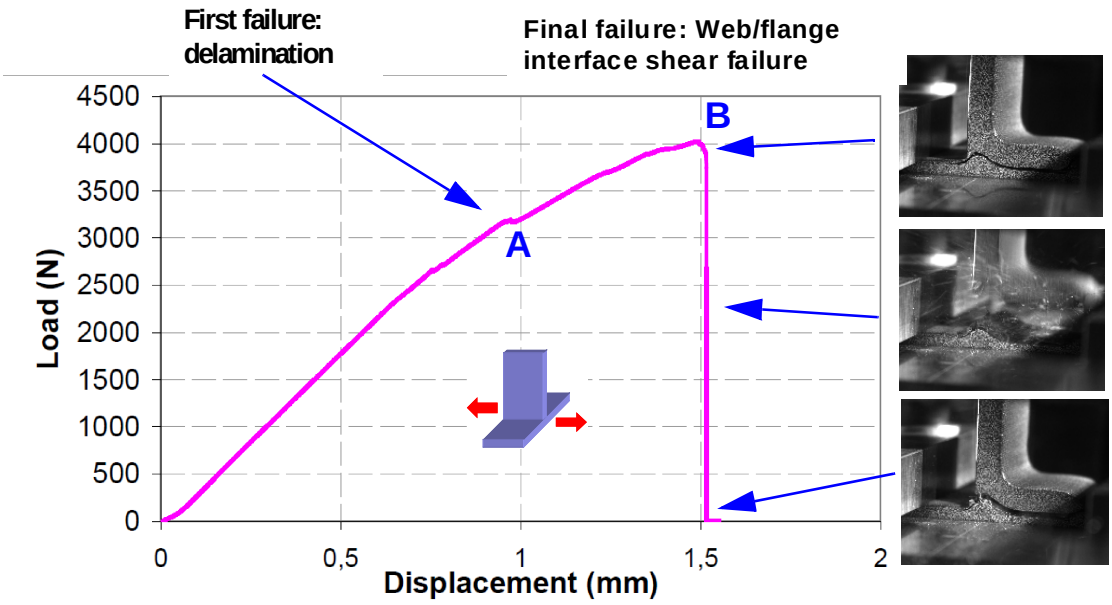

Figure N°17: Typical shear L-joint behaviour .

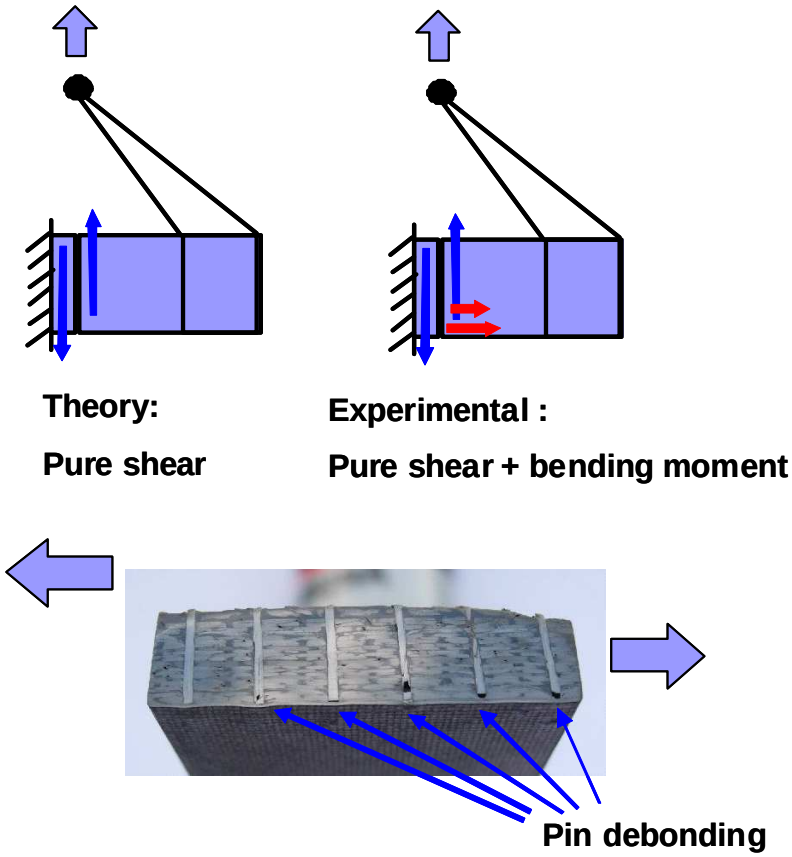

Figure N°18: Failure scenario and real loading in s hear.

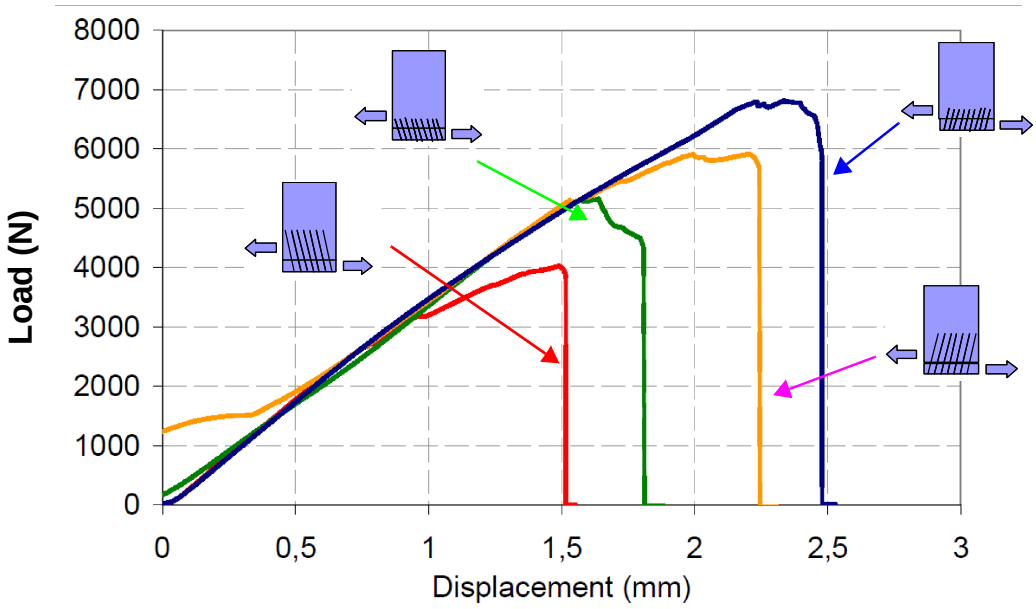

Figure N°19: Load/displacement curves for T pinned joints under shear.

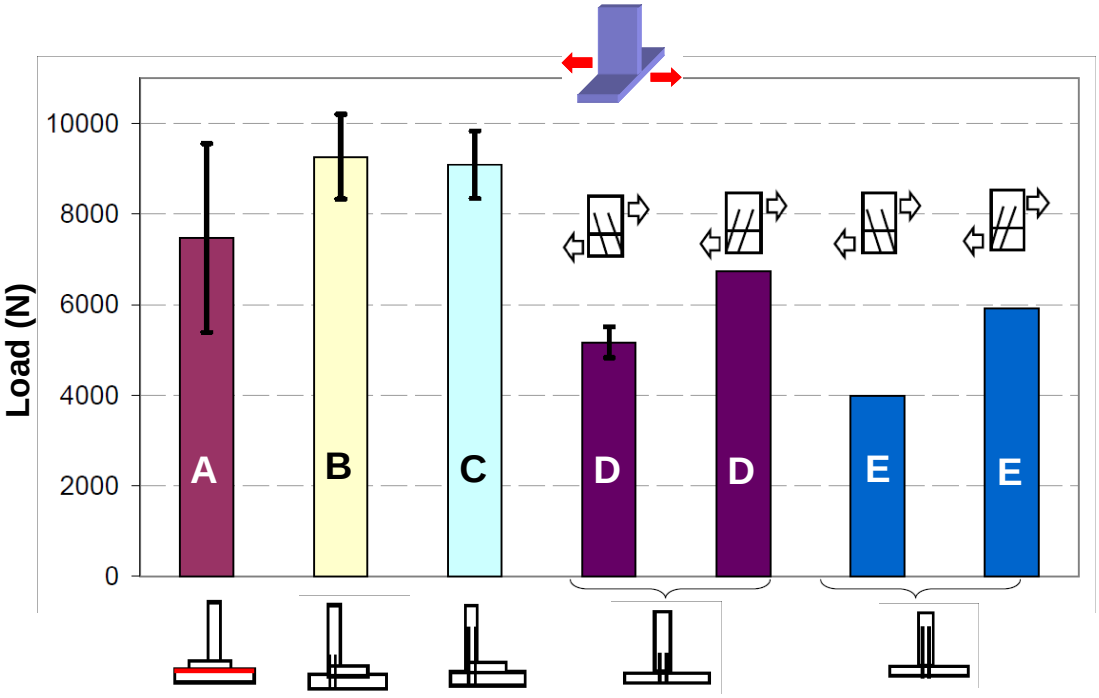

Figure N°20: Shear maximum applied load for L and T-joints.

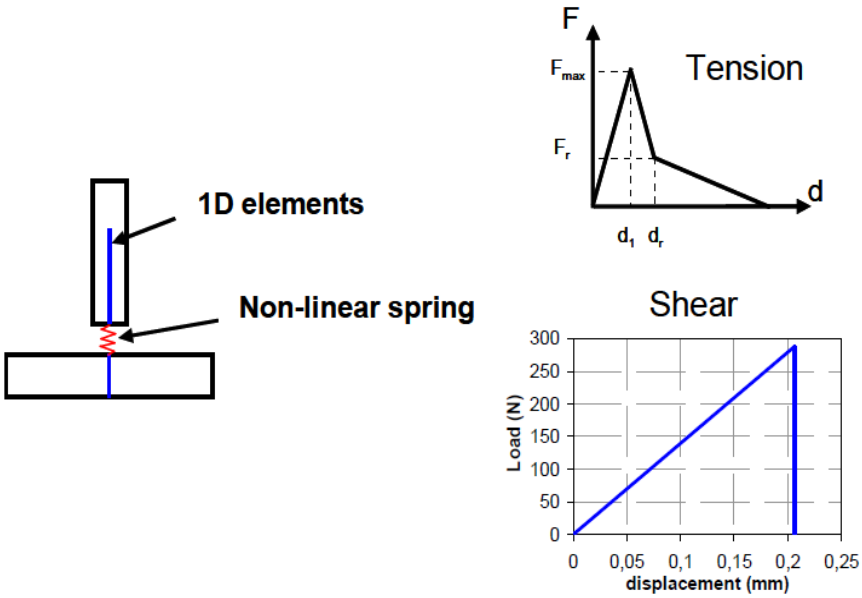

Figure N°21: Modelling principle.

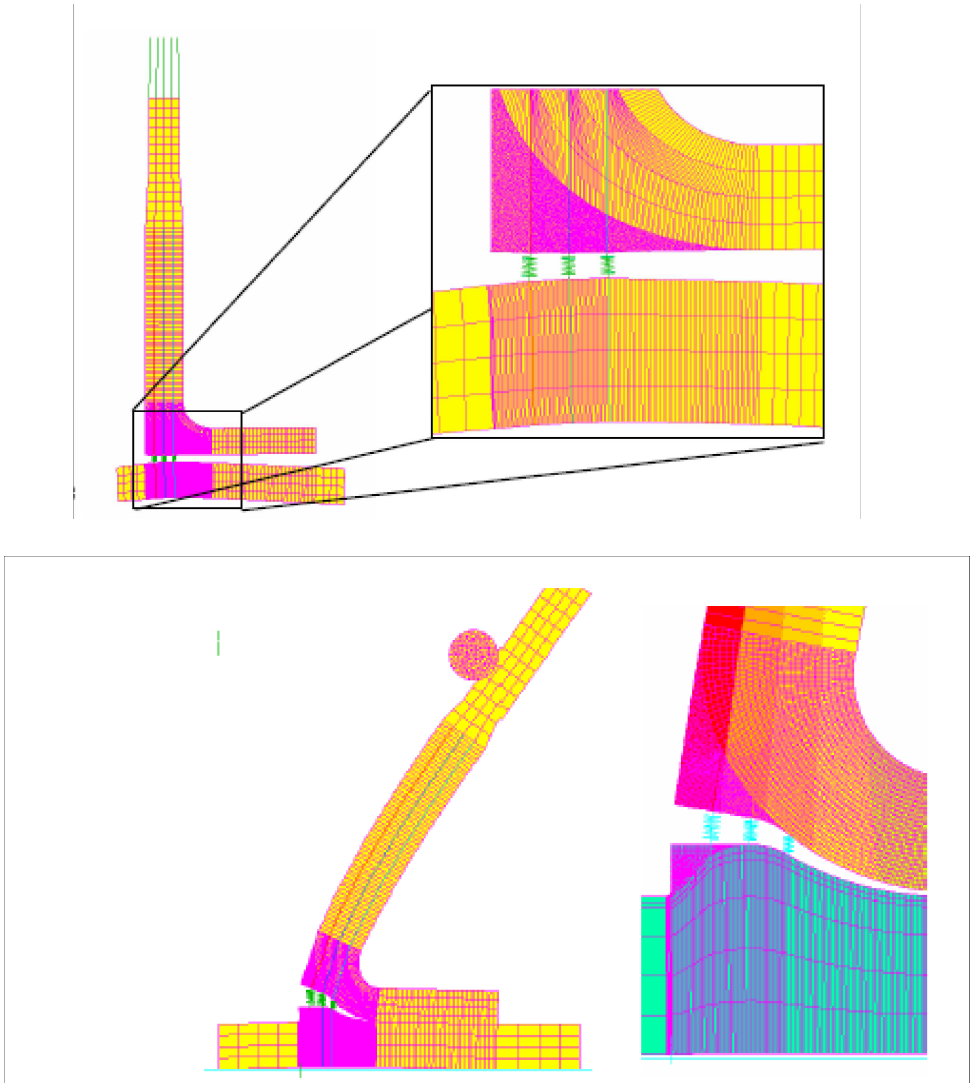

Figure N°22: L-joint FE model for tension (up) and bending (down).

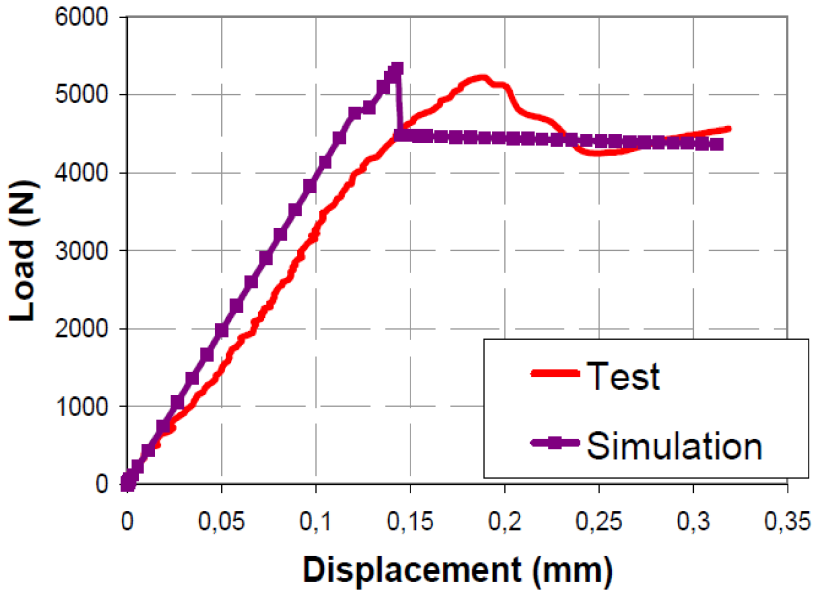

Figure N°23: Test/computation comparison for pinned L-joint under tension.

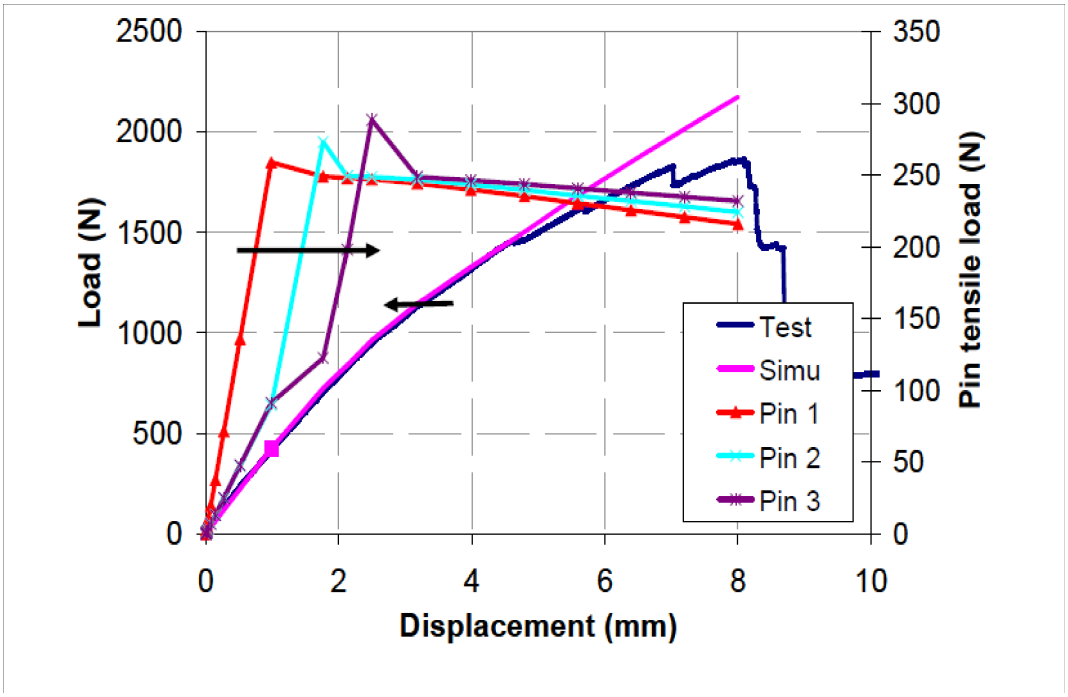

Figure N°24: Test/computation comparison for pinned L-joint under bending.

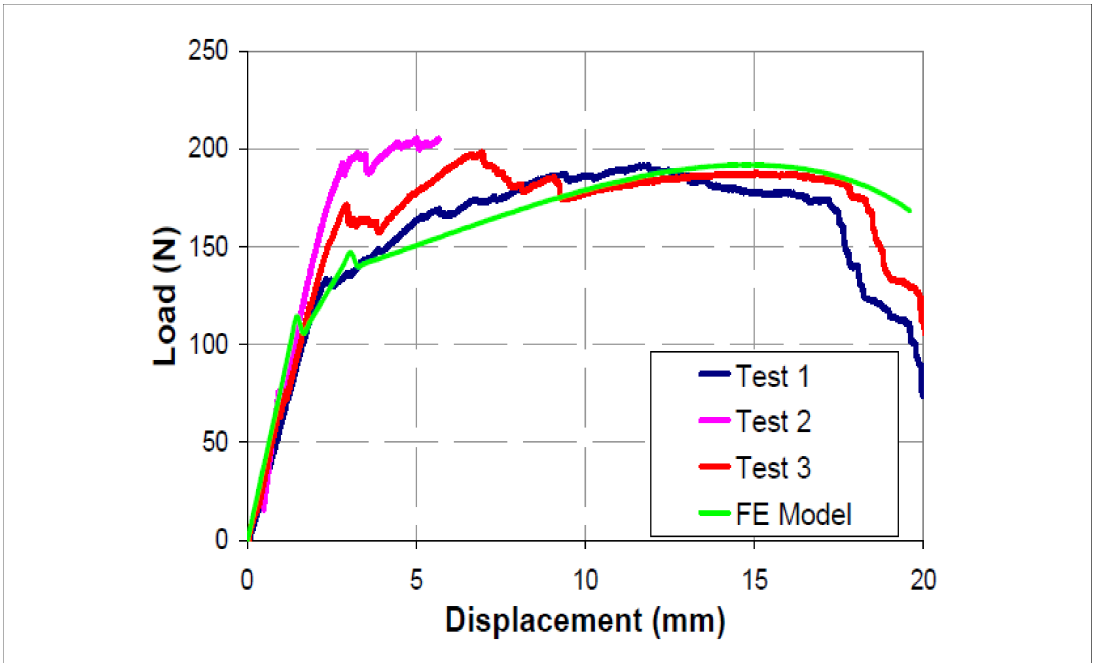

Figure N°25: Test/computation comparison for pinned T-joint under bending.

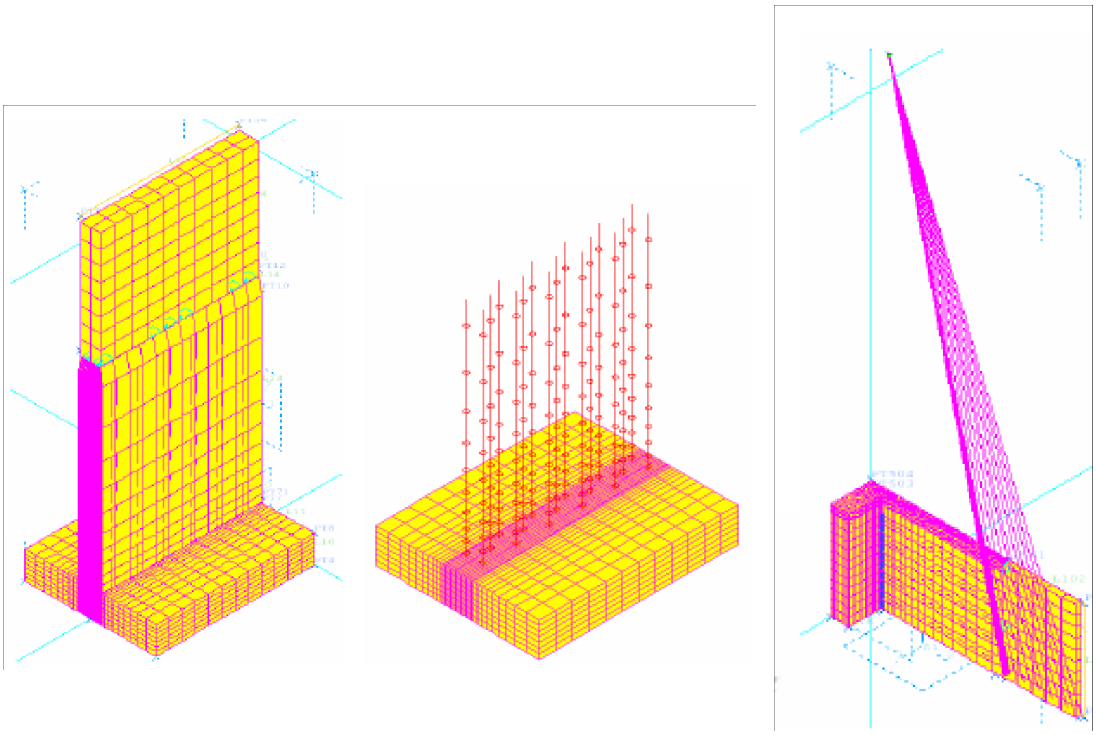

Figure N°26: T-joint F.E. model under shear.

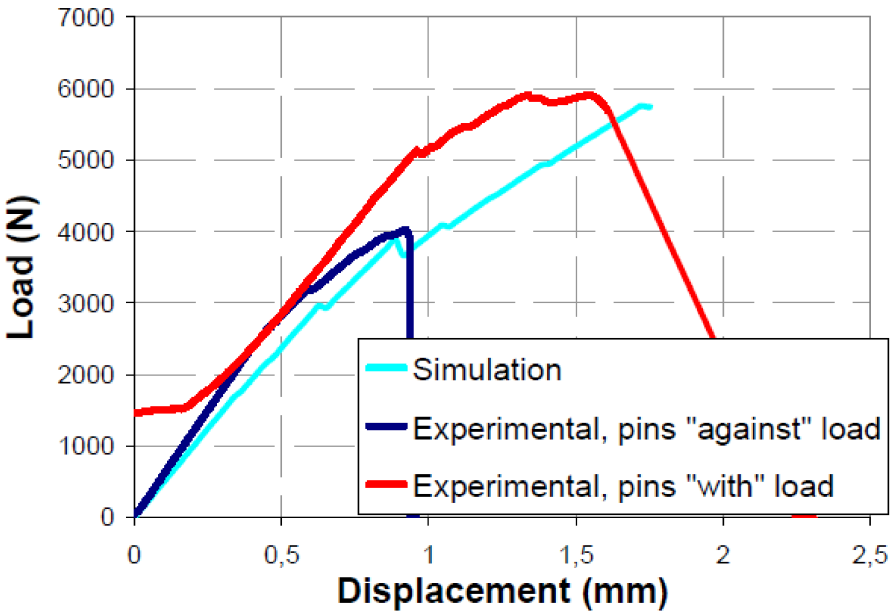

Figure N°27: Test/computation comparison for pinned T-joint under shear.

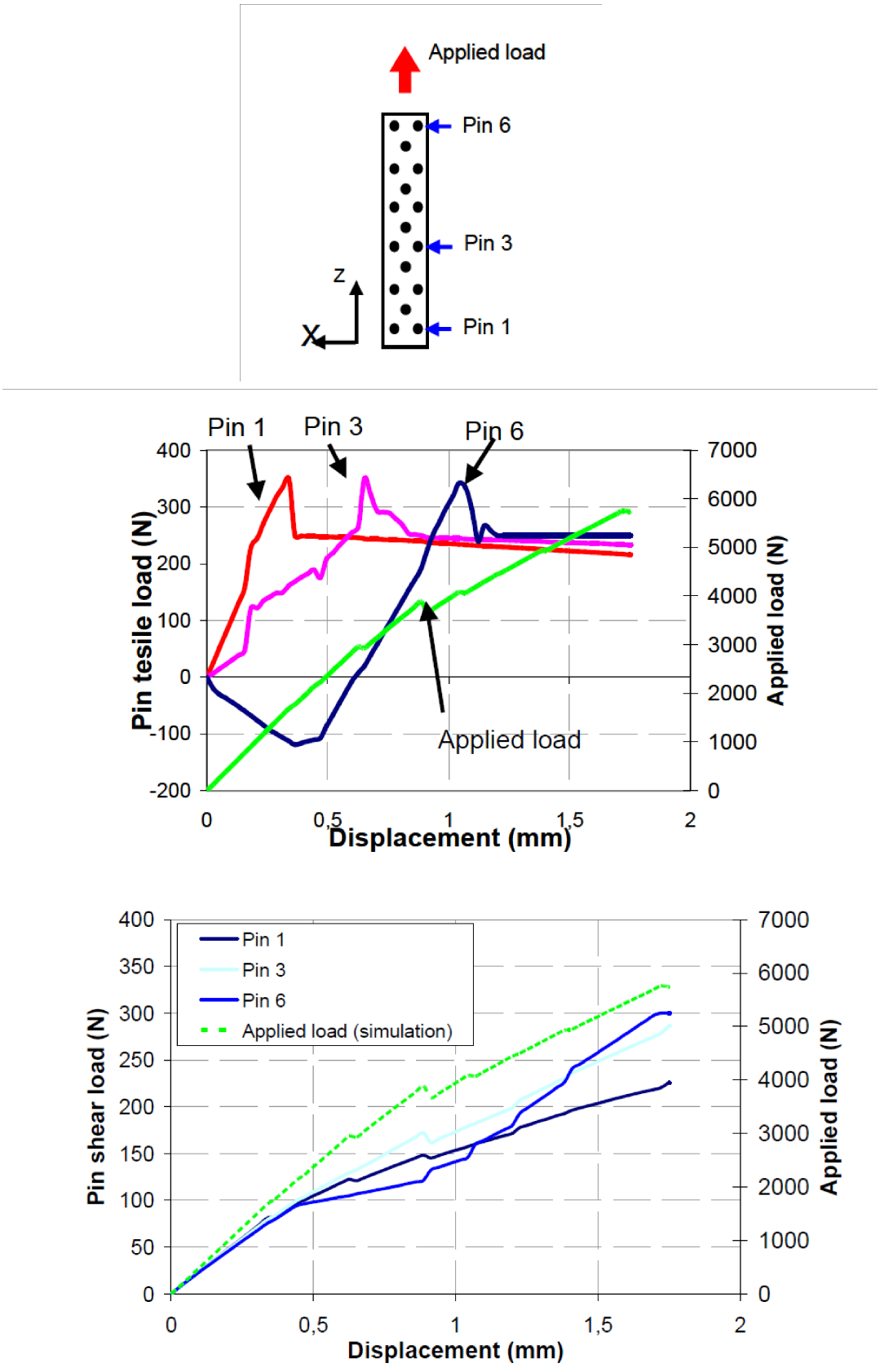

Figure N°28: Pins axial and shear evolution for pin ned T-joint under shear.

TABLES

	E1 (MPa)	Et = Ez (MPa)	ν_{lt}	Glt (MPa)
Skin plies	145000	9000	0,32	4500
Rib-foot plies	84000	8300	0,32	3800

Table 1